

Depth measurements of etch-pits in GaN with shape reconstruction from SEM images

M. WZOREK*, A. CZERWINSKI*, J. RATAJCZAK*, A. LUI†, E. IACOB† & J. KATCKI*

*Institute of Electron Technology, Warsaw, Poland

†Fondazione Bruno Kessler, Trento, Italy

Key words. Etching, GaN, SEM, shape-from-shading.

Summary

The method, which allows shape reconstruction by reading the intensity from the scanning electron microscopy image, is presented and discussed in details. The method is applied to read the morphology of etch-pits, which were formed on the GaN surface by etching in molten KOH–NaOH eutectic mixture to delineate dislocations. The etch-pit depth distributions are obtained and used to determine densities of pits related to screw, mixed or edge-type dislocations. The results are compared with atomic force microscopy.

Introduction

GaN epitaxial layers have a large density of threading dislocations. The line of a threading dislocation lies along (0001) direction and considering its Burgers vector, threading dislocation can be one of the three types. Edge-type dislocation has its Burgers vector of a type $(1/3)\langle 2 -1 -1 0 \rangle$, the Burgers vector of screw type dislocation is $\langle 0 0 0 1 \rangle$ and the mixed type has its Burgers vector of a type $(1/3)\langle 2 -1 -1 3 \rangle$. The influence of a dislocation on the device properties can depend on the dislocation type. Chemical etching is a convenient method to estimate dislocation densities. The morphology of etch-pits in GaN depends on the dislocation type (Weyher *et al.*, 2007). It should be possible to assign a given etch-pit to appropriate dislocation type basing on the analysis of pit morphology. However, simple measuring of lateral sizes of etch-pits is not satisfactory because it does not take into account the observed differences in inclination angles of the facets (Weyher *et al.*, 2007; Wzorek *et al.*, 2009), which are dependent on dislocation type. A quantitative method was proposed previously (Wzorek *et al.*, 2009), which is based on processing of scanning electron microscopy (SEM)

micrographs and can be used to reconstruct profiles of the etch-pits. In this work, an improved experimental setup was applied, that is, with the microscope equipped with a field-emission gun and an in-lens detector. The obtained depth distributions were compared with the results of atomic force microscopy (AFM).

Experimental details

The samples of p-type (0001) GaN layer, which had been grown by metal-organic vapour phase epitaxy on a sapphire substrate were subjected to selective etching in a KOH–NaOH eutectic mixture at various temperatures and with various etching times to delineate dislocations. The sample with best etching conditions, from which the results are presented, had been etched at 455°C for 10 min. Etching was performed in a Ni crucible and the temperature was measured with a thermocouple inside the aluminium plate on which the crucible was placed. The etched sample was examined in JEOL JSM-7401F scanning electron microscope, at 20 kV accelerating voltage. The AFM analysis was performed using NT-MDT Solver PRO SPM equipment.

Shape reconstruction method

The secondary electron emission dependence on the electron beam incident angle α can be described by: $\delta_\alpha = \delta_0 \exp[p(1 - \cos\alpha)]$ (Bruining, 1938), where δ_0 describes emission for $\alpha = 0$, when the electron beam direction is perpendicular to the surface. The parameter p depends on the material and the electron energy. However, the equation cannot describe the image intensity recorded in the SEM image, where microscope settings additionally affect the brightness and contrast of the image. A simple modification was proposed previously (Wzorek *et al.*, 2009) to obtain the model for image intensity dependence on surface slope which can be applied to SEM images:

$$I = A \exp[p(1 - \cos \alpha)] + B, \quad (1)$$

Correspondence to: M. Wzorek, Institute of Electron Technology, al. Lotników 32/46, 02-668 Warsaw, Poland. Tel: +48-22-5487895; fax: +48-22-8470631; e-mail: mwzorek@ite.waw.pl

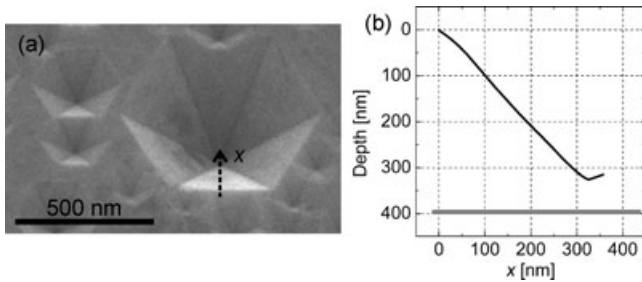


Fig. 1. (a) SEM image of exemplary pits. The sample was tilted 30° . The dashed line represents direction used to obtain the profile presented in (b). The profile includes correction of the tilt angle. The horizontal line in (b) represents the depth of the pit determined with stereogrammetry method.

where I denotes the image intensity, A and B are parameters which describe microscope settings that affect image contrast and brightness. Equation (1) can be rewritten in the form $\alpha = \arccos[1 - (1/p)\ln((I - B)/A)]$. When parameters A , B and p are known, the angles α , determined from SEM image intensities I , can be applied to calculate the pit profile by applying simple geometric calculations. However, the direction which is used to extract the profile from the image should be chosen carefully so that the angle α should describe the surface slope along this direction. In Fig. 1(a), the direction that can be used to obtain a profile from an SEM image of a pit is marked as a dashed line.

There are some limitations of Eq. (1) that should be discussed. The collection efficiency of the secondary electrons (SEs) at the detector can be different for different parts of the sample. In this work, the microscope with the in-lens detector is used, which is supposed to minimize the shadowing effect.

Another phenomenon is the contribution of backscattered electrons to the SE emission. Although only those SEs which are generated very close to the surface have sufficient energy to leave the sample, the BSEs can generate additional SEs near the surface (SE2 electrons), and furthermore can again hit the sample in another place and generate SE3 secondary electrons (e.g. Reimer, 1998). The SE2 and SE3 contributions make the dependence of SE emission on surface morphology more complicated than Eq. (1). This situation is schematically presented in Fig. 2(a).

The measurements of angular distribution of backscattered electrons (Darliński, 1981) indicate that for large incident angles the most part of the backscattering is 'reflection-like'. It implies that most of the backscattered electrons will generate SE3 at the opposite sidewall of the pit which will contribute to the signal at the detector. To verify whether in this particular case the resultant image-intensity, which is related to SE1 as well as to BSE contributions to SE emission, can be described with the Eq. (1), the following experimental procedure was performed.

Inclinations of the sidewalls for a set of various pits were determined with SEM using the stereogrammetry method (e.g. Reimer, 1998) with 0° and 30° tilt stereo-pair images.

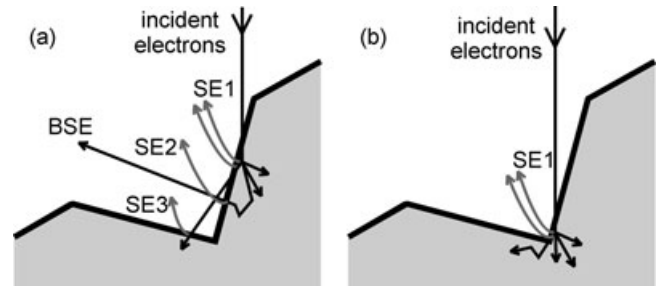


Fig. 2. Schemes of an exemplary pit and contributions to the secondary electron emission for two positions of the electron beam. SE1 – electrons generated by the incident beam, SE2 – electrons generated by backscattered electrons leaving the sample, SE3 – electrons generated at another parts of the specimen by backscattered electrons which hit again the sample.

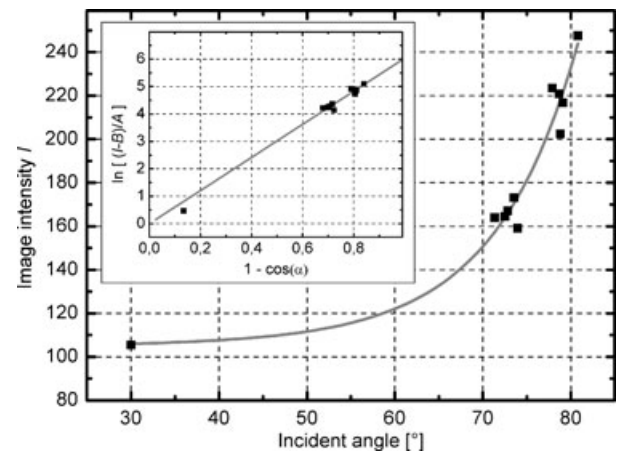


Fig. 3. SEM image intensity I versus electron beam incident angle α . The angles are etch-pit sidewalls inclination angles determined with stereogrammetry plus 30° specimen tilt angle. The curve represents the fit of Eq. (1) to the experimental points. The point at 30° represents flat surface of the sample. The inset presents the same experimental points and the model in the plot of $\ln[(I - B)/A]$ versus $1 - \cos\alpha$.

The corresponding image intensities – taken as average pixel values of the sidewalls – were read from the 30° image. The results are presented in Fig. 3, where image intensity is plotted versus electron beam incident angle. The curve in the figure represents fitted model given by Eq. (1). The inset in the figure presents the values of $\ln[(I - B)/A]$ as a function of $(1 - \cos\alpha)$, where A and B are fitted parameter values. It can be seen that Eq. (1) fits the experimental points rather well.

At least three experimental points with different values of α are needed to calculate three parameters of the model using the stereogrammetry method. It is important that the determined values of the parameters obtained from one area can be applied afterward for analysis with the shape reconstruction method of any single SEM image that is obtained with the same temporary microscope settings. This is the advantage

over the stereogrammetry itself, which requires, besides more complicated calculations, two images of every examined area.

Results and discussion

An example of the profile extracted from the SEM image is shown in Fig. 1(b). The horizontal line represents the depth of the pit calculated using stereogrammetry. Such a comparison was made for the set of various pits. The depths obtained from the extracted profiles using the shape-reconstruction

method are equal to about 80–90% of the values obtained with stereogrammetry. The slightly lower depths are related to the decrease in image intensity in the vicinity of the bottom of the pits. When comparing these results with the results presented in the previous paper (Wzorek *et al.*, 2009), which were obtained with the detector placed in the microscope chamber, it can be seen that the in-lens detector did not eliminate these decrease in image intensity. Hence, not only the electron collection efficiency might be responsible for this decrease. Another possible explanation is illustrated in Fig. 2.

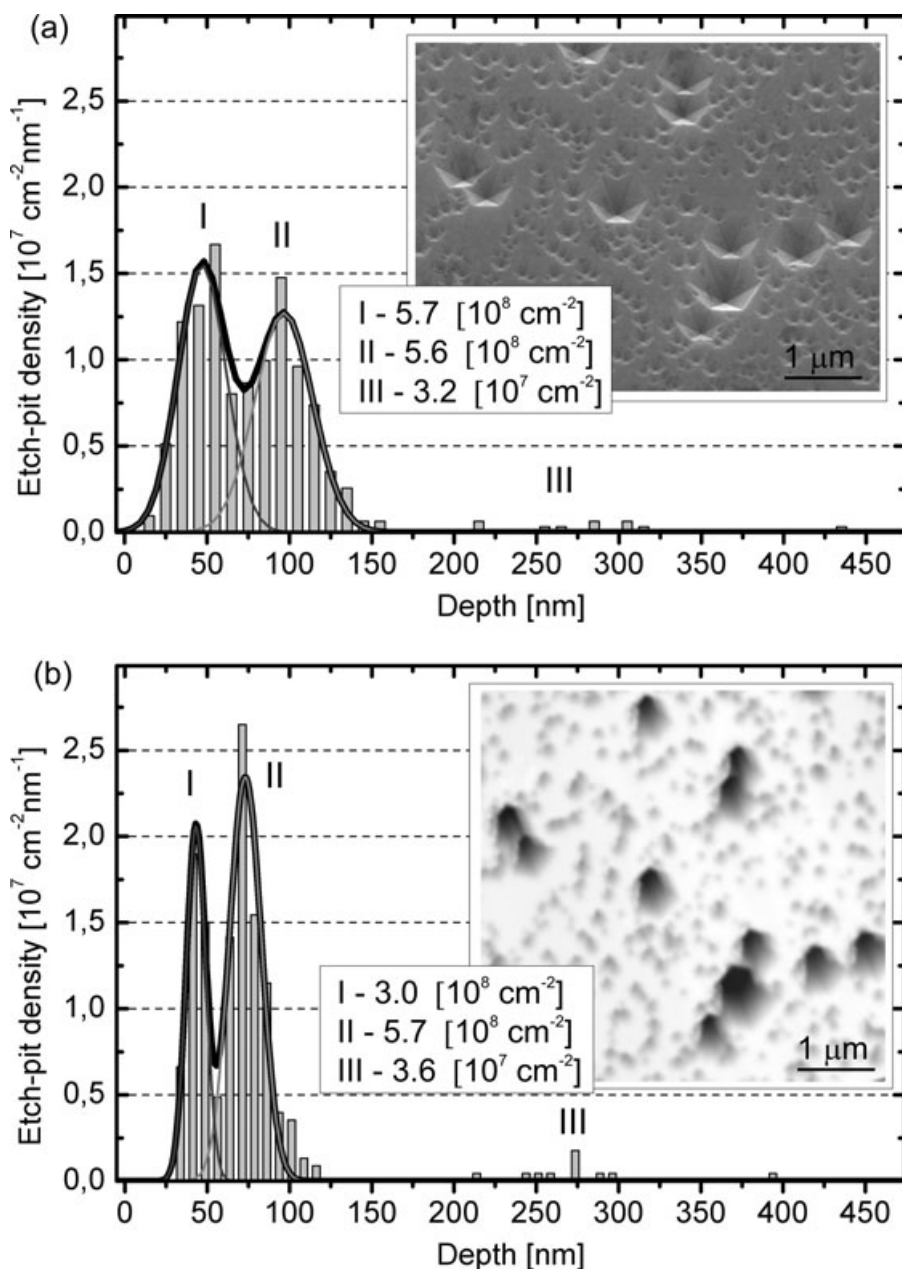


Fig. 4. Histograms of etch-pit depth distributions obtained from (a) SEM image and (b) AFM image of the same area of the sample. The corresponding images are shown in the insets.

The contribution of backscattered electrons to generation of SE2 and SE3 electrons is decreasing when approaching the bottom of the pit, which can explain the observed decrease in image intensity.

The presented method was used to obtain the etch-pit depth distribution from an SEM image. The area of $31 \mu\text{m}^2$ was examined and 365 etch-pits were analysed. Etching in KOH–NaOH eutectic mixture results in the formation of hexagonal pits, which are oriented along parallel crystallographic directions [Weyher *et al.*, 2007] and hence, all of the pits can be appropriately oriented in the microscope chamber at the same time and their profiles can be determined. Another, separated problem is the algorithm that can find positions of the pits in the image automatically. For example, a kind of water-shed algorithm can be used for this aim, however the experiments that has been performed so far, required some further correction of the algorithm output by the user. The etch-pit depth distribution that was obtained with the presented method is shown in Fig. 4(a). Two peaks in the range from 0 to 150 nm are clearly visible as well as a deeper part of the distribution can be separated in the depth range up to 450 nm. The smallest pits are expected to form at edge-type dislocations (Weyher *et al.*, 2007), therefore the peak of the shallowest pits in the distribution can be attributed to this type of dislocations. Similarly, the peak in the medium depth range should be related to mixed dislocations and the deepest part of the distribution to screw-type dislocations.

For comparison, an AFM scan of exactly the same area of the sample was performed. The AFM image and the resultant depth distribution is presented in Fig. 4(b). The densities of pits determined with SEM related to mixed dislocations and to screw-type dislocations are close to the values determined with AFM. However, the density of the pits related to edge-type dislocations determined from the SEM image is larger than that obtained from AFM. The resolution of the SEM image in this particular case is better than in the AFM image and more of the smallest pits can be resolved. It is also confirmed by the overall density of etch pits, which is higher if determined with SEM ($1.2 \times 10^9 \text{ cm}^{-2}$ for SEM and 9.1×10^8 for AFM). This difference is even higher if it is taken into account that some part of the pits were omitted in the calculations due to

overlapping of the pits, which would lead to underestimated values of calculated depths. Comparing the distributions from Fig. 4, it can be seen that depths measured with SEM are larger than that obtained with AFM. The AFM data is a convolution of the shape of the pit and the shape of the feature imaged. The depths obtained with stereogrammetry, which are even larger than that obtained with shape-reconstruction method (Fig. 1), prove that in this particular case the depth measurements with AFM are less accurate. Nevertheless, the AFM examination confirmed the presence of three peaks in the depth distribution which can be assigned to different dislocation types.

Conclusions

Depth distributions of etch-pits obtained with the presented method were compared with the AFM technique. It was shown that the presented method, which uses secondary electron emission model for the shape reconstruction from SEM images, produces reliable results.

Acknowledgements

This work was supported by the European Commission – Research Infrastructure Action under the FP6 ‘European Integrated Activity of Excellence and Networking for Nano and Micro-Electronics Analysis’ – Project number 026134(RI3) ANNA.

References

- Bruining, H. (1938) Secondary electron emission part II. Absorption of secondary electrons. *Physica* **V**, 901–912.
- Darliński, A. (1981) Measurements of angular distribution of the backscattered electrons in the energy range of 5 to 30 kV. *Phys. Stat. Sol. A* **63**, 663–668.
- Reimer, L. (1998) *Scanning Electron Microscopy: Physics of Image Formation and Microanalysis*, 2nd edn. Springer-Verlag, Berlin.
- Weyher, J.L., Lazar, S., Macht, L., *et al.* (2007) Orthodox etching of HVPE-grown GaN. *J. Cryst. Growth* **305**, 384–392.
- Wzorek, M., Czerwinski, A., Ratajczak, J., Dylewicz, R. & Kątcki, J. (2009) Selective etching of dislocations in GaN and quantitative SEM analysis with shape-reconstruction method. *Micron* **40**, 37–40.